Published in final edited form as:
Heart Rhythm. 2009 September ; 6(9): 1318–1326. doi:10.1016/j.hrthm.2009.05.016.

A novel *SCN5A* mutation V1340I in Brugada syndrome augmenting arrhythmias during febrile illness

Kaveh Samani, MD[*], **Geru Wu, MD, PhD**[*,†], **Tomohiko Ai, MD, PhD**[*,†], **Mossaab Shuraih, MD**[*], **Nilesh S. Mathuria, MD**[*], **Zhaohui Li, PhD**[‡], **Yoshiro Sohma, MD, PhD**[§,□], **Enkhsaikhan Purevjav, MD, PhD**[‡], **Yutao Xi, PhD**[*], **Jeffrey A. Towbin, MD, FAAP, FACC**[‡], **Jie Cheng, MD, PhD, FACC, FHRS**[*], and **Matteo Vatta, PhD**[‡]

[*]Electrophysiology Research Laboratory, Texas Heart Institute/St. Luke's Episcopal Hospital, Houston, Texas

[†]Pharmacology/Osaka Medical College, Takatsuki, Osaka, Japan

[‡]Pediatric Cardiology, Texas Children's Hospital/Baylor College of Medicine, Houston, Texas

[§]Department of Pharmacology/Keio University School of Medicine, Tokyo, Japan

[□]Dalton Cardiovascular Research Center/University of Missouri-Columbia, Columbia, Missouri

Abstract

BACKGROUND—Mutations in the *SCN5A* gene, which encodes the cardiac sodium channel, have been implicated in the pathogenesis of Brugada syndrome (BrS). Febrile illnesses have been recognized to unmask and/or trigger the BrS phenotype. However, the patho-physiological mechanism has not been fully elucidated.

OBJECTIVE—A novel *SCN5A* missense mutation, V1340I, was identified in a patient with BrS suffering from frequent episodes of polymorphic ventricular tachycardia (VT) and syncope associated with fever. The biophysical modifications of $hNa_v1.5$ by V1340I were studied.

METHODS—The effects of the V1340I mutation were studied in the 2 splice variants, SCN5A and SCN5A-Q1077del (delQ), using patch-clamp techniques at various temperatures between 22°C and 40°C.

RESULTS—At 22°C, V1340I-SCN5A generated markedly diminished sodium currents compared to the wild-type (WT) SCN5A. On the contrary, V1340I-delQ generated almost identical current density compared to the WT-delQ. However, V1340I-delQ significantly attenuated the peak current density compared to the WT-delQ at 32°C, 37°C and 40°C. The voltage dependency of steady-state activation was leftward shifted both in WT-delQ and V1340I-delQ at 40°C. In addition, the V1340I-delQ accelerated the recovery time course from fast inactivation compared to the WT-delQ at 40°C. Immunohistochemical staining showed that both V1340I-SCN5A and V1340I-dQ were expressed in the plasma membrane.

Address reprint requests and correspondence: Dr. Matteo Vatta, Department of Pediatrics (Cardiology), Baylor College of Medicine/ Texas Children's Hospital, 1102 Bates Street, F.C. 430.04, Houston, Texas 77030. mvatta@bcm.tmc.edu. Drs. Ai or Cheng, Electrophysiology research laboratory, Texas Heart Institute/St. Luke's Episcopal Hospital 6770 Bertner Ave. MC 2-255 Houston, Texas 77030. tomohikoaiat@yahoo.com; jcheng@heart.thi.tmc.edu.
Drs. Samani, Wu, and Ai contributed equally to this work.

This work was presented in part at the 51st Annual Meeting of Biophysical Society in Baltimore, Maryland, March 2007.

CONCLUSION—Our study supports the concept that febrile illness predisposes individuals who carry a loss of function SCN5A mutation, such as V1340I, to fever-induced ventricular arrhythmias in BrS by significantly reducing the sodium currents in the hyperthermic state.

Keywords

Brugada syndrome; Severe; Arrhythmia; Sodium channel; Mutation

Introduction

Brugada syndrome (BrS) is a primary arrhythmogenic disease that can cause sudden cardiac death in young populations.[1–3] It is inherited as an autosomal dominant trait,[4] with approximately 20% of BrS cases caused by mutations in the *SCN5A* gene that encodes the α-subunit of the cardiac sodium channel. Electrophysiological studies using animal models and mammalian cell lines have suggested that reduced sodium currents account for loss of the epicardial action potential (AP) dome, which may lead to the exaggeration of the transmural AP dispersion in the right ventricular outflow tract and gives rise to the typical ST-segment elevation in the right precordial electrocardiogram (ECG) leads.[5–7] Recent studies also revealed that anisotropic conduction due to the structural abnormality in the right ventricular outflow tract might contribute to the formation of phase 2 reentrant tachycardia circuits.[8,9]

BrS phenotypes vary depending on a variety of factors, such as gender, ethnicity, and age, even among individuals who carry the same genetic mutation. In addition, several conditions that can affect various ion channel functions have been identified, which result in variable BrS clinical manifestations.[5,6,10,11] Previous case reports have shown that high body temperature can unmask or promote the BrS phenotypic ECG changes and ventricular arrhythmias.[12–21] Electrophysiological studies using in vitro cell expression systems have shown that the increase of temperature going from ambient temperature to high temperature (32°C to 41°C) can decrease sodium currents by altering ion channel gating kinetics.[18–21]

Here we report a BrS patient with worsening arrhythmic episodes only during febrile illness in whom genetic analysis identified a novel nucleotide change in *SCN5A* (4018G>A) resulting in the amino acid substitution of valine to isoleucine at position 1340 (V1340I). The electrophysiological characteristics of the V1340I were studied and compared to the wild-type (WT) channel using 2 major alternatively spliced and ubiquitously expressed SCN5A transcripts, namely the 2016 amino acid encoding transcript containing Q1077 (annotated here as SCN5A) and the 2015 amino acid encoding transcript lacking Q1077 (annotated here as SCN5A-Q1077del or delQ).[22]

Methods

Clinical manifestation

A 37-year-old Caucasian male was referred to Texas Children's Hospital for the genetic diagnosis of BrS. At 29 years of age, the patient was admitted to a local hospital with a diagnosis of pneumonia and had 2 episodes of aborted sudden cardiac death during high fever (101.6° F). He was successfully resuscitated and recovered from a coma 2 days after the attack. Three days after the events, he underwent an electrophysiological study, ultimately resulting in the patient receiving an automated implantable cardioverter-defibrillator (ICD). Polymorphic ventricular tachycardia (VT) and ventricular fibrillation (VF) were induced by programmed stimulation during the electrophysiological study (data not shown). The patient's ECG taken at afebrile state showed Brugada-type ST-segment change (Figure 1, type I). At 32 years of age, he had multiple ICD discharges (>15 times) due to frequent VT/VF during a febrile disease. The patient had no documented family history of BrS, sustained ventricular arrhythmias, or

sudden death. His parents were seemingly healthy, and their baseline ECGs were normal. Pharmacological provocation tests were not performed on his parents due to their wills.

SCN5A mutational analysis—Blood samples were collected after informed written consent was obtained from the subjects who participated in the study. Genomic DNA was extracted from peripheral blood lymphocytes, as previously described.[23] Using polymerase chain reaction, denaturing high-performance liquid chromatograph, and direct DNA sequencing, open reading frame/splice site mutational analysis using coding region flanking primers was performed on *SCN5A*, the most common BrS-associated gene, but not on the other 5 minor genes.

Cell culture and transient expression of sodium channels—To express WT or V1340I channels, HEK-293 cells were grown in Dulbecco modified Eagle medium supplemented with 10% fetal bovine serum (FBS) in a CO_2 incubator (37°C). The plasmid pcDNA3.1 (5 μg) containing either WT-SCN5A, WT-delQ, V1340I-*SCN5A*, or V1340I-delQ cDNA was co-transfected with pEGFP-C3 (0.5 μg; Clontech, Mountain View, California) encoding green fluorescent protein or with pIRES containing human sodium channel β_1-subunit ($h\beta_1$) and CD8 cDNA (kindly provided by Dr. Naomasa Makita, Hokkaido University, Sapporo, Japan) using Lipofectamine 2000 transfection reagents (Qiagen, Valencia, California). The cells were incubated at 37°C for 48 to 72 hours before use.

Patch-clamp experiments

Patch-clamp experiments were performed following the method described previously.[23] Briefly, step-pulse voltages were generated by an Axopatch 200B amplifier with Pclamp 9 software (Axon Instruments, Sunnyvale, California). Currents were filtered at 10 kHz with a built-in 4-pole Bessel filter and then fed to a computer (OptiPlex GX260, Dell) at 20 kHz. The pipette solution contained 10 NaF, 110 CsF, 20 CsCl, 10 EGTA, and 10 HEPES (in mM, pH 7.35 with CsOH). Bath solution contained 145 NaCl, 4 KCl, 1 $MgCl_2$, 1.8 $CaCl_2$, 10 HEPES, and 10 glucose (in mM, pH 7.35 with NaOH). Chamber temperature was precisely controlled with PH-1 heating platform, SH-27B solution heater, and TC-344B temperature controller (Warner Instruments, Hamden, Connecticut). The temperature reached steady state in approximately 2 minutes after temperature setting change. Hyperthermic effects on the V1340I's gating kinetics parameters were studied and compared with the WT at 22°C and 40°C. The effects of V1340I on the current amplitudes were also studied at 22°C, 32°C, and 37°C in same cell using a −25 mV depolarization pulse protocol.

Immunostaining

Immunohistochemistry was performed using standard techniques described previously.[23] Briefly, HEK-293 cell lines were transfected with the FLAG-tagged V1340I-delQ or V1340I-SCN5A and selected with Geneticin for 3 weeks at 37°C. The surviving cells were plated on poly-D-lysine coated cover slips and fixed with 4% formaldehyde. The fixed cells were incubated in 1 mg/ml $NaBH_4$, then incubated with 0.5% Triton X-100. The treated cells were sequentially stained with monoclonal anti-FLAG antibody (1:500 dilution, Sigma-Aldrich, St. Louis, Missouri) and FITC-conjugated anti-mouse immunoglobulin G (1:500 dilution, Sigma-Aldrich) either at room temperature or at 37°C. Nonspecific binding was blocked with 1% (w/v) bovine serum albumin in phosphate-buffered saline–Tween (0.1%, Tween-20). Fluorescence images were obtained using a TCS-SP2 confocal laser-scanning microscope (Leica Microsystems, Bannockburn, Illinois).

Data analysis

Whole-cell current amplitude and gating kinetics were analyzed using Clampfit (Axon Instruments), Origin (OriginLab, Northampton, Massachusetts), Igor software (Wavemetrics, Lake Oswego, Oregon), and SPSS 13.0 (SPSS Inc., Chicago, Illinois). Data were presented as mean ± SD unless otherwise stated. Comparisons among data were made using Mann-Whitney-Wilcoxon test or ANOVA followed by Tukey test with $P < .05$ considered statistically significant.

Results

Mutational analysis

Mutation screening of genomic DNA from the proband and his father identified an abnormal conformer in the exon 23 of *SCN5A*. DNA sequencing revealed a heterozygous 4018G>A nucleotide change resulting in a conservative amino acid substitution from valine to isoleucine at position 1340 (V1340I) (Figure 2A). The patient's mother was negative for the V1340I mutation (Figure 2B). In addition, other SCN5A polymorphisms such as H558R were not identified in any of the analyzed subjects.

The sodium channel gating kinetics were similar between WT and V1340I in the SCN5A-delQ background at 22°C

Electrophysiological studies using heterologous expression systems have shown that sodium channel gating kinetics may be affected by background variations.[22,24] V1340I gating kinetics were first studied in the SCN5A-delQ background at 22°C. Figure 3A shows superimposed current traces obtained from the cells expressing WT-delQ or V1340I-delQ. Figure 3B shows the current-voltage (I–V) relationships. The peak current densities were almost identical between WT-delQ and V1340I-delQ. The normalized conductance and the normalized peak currents obtained by the pre-pulse protocols were plotted as a function of membrane potentials (Figure 3C) and the data were fitted with the Boltzman equation to calculate the half-maximal voltages (V_h) and the slope factors (k). The voltage dependency of the steady-state activation and inactivation were comparable between WT-delQ and V1340I-delQ at 22°C (Table 1).

V1340I markedly reduced sodium currents in the *SCN5A* background

Next, V1340I currents were studied in the SCN5A background. Figure 3D shows superimposed current traces obtained from the cells expressing WT-SCN5A or V1340ISCN5A. WT-SCN5A generated significant currents by a step-pulse protocol from a holding potential of −140 mV (Figure 3D upper panel; peak current amplitude: 308.2 ± 68.0 pA/pF, n = 6). On the contrary, V1340I-SCN5A did not show significant currents (n = 12), or generated very small currents (Figure 3D lower panel; peak current amplitude: <10 pA/pF, n = 2), which might be the endogenous sodium currents of HEK-293 cells.

To examine whether V1340I-SCN5A channels are expressed in the plasma membrane, the cells stably transfected with FLAG-tagged V1340I-SCN5A (FLAG was inserted in the cytoplasmic loop S_2S_3 of domain I) or FLAG-tagged V1340I-delQ were fixed and stained with anti-FLAG antibody. Figure 3E shows the fluorescence images of the stained cells. The plasma membrane of the cells transfected with both V1340I-delQ and V1340I-SCN5A shows significant staining. These results indicate that V1340I-SCN5A channels are essentially nonfunctional.

V1340I-delQ attenuated the sodium currents at hyperthermic state

To mimic the hyperthermic state, the gating kinetics of V1340I-delQ were studied and compared to the WT at 40°C. Figure 4A shows the superimposed current traces obtained from

the cells transfected with WT-delQ or V1340I-delQ at 40°C. The current decays of peak currents at 40°C were substantially faster than at 22°C in both WT-delQ and V1340I-delQ constructs (Table 1). Figure 4B shows the I–V relationships, with the peak current density being significantly reduced in the cells expressing V1340I-delQ compared to the WT-delQ at 40°C (Figure 4B). Figure 4C shows the voltage dependency of steady-state activation and inactivation. The voltage dependency of the steady-state activation was leftward shifted both in the cells expressing WT-delQ and V1340I at 40°C (Table 1). Cotransfected hβ_1-subunit did not affect the gating kinetics of either WT-delQ or V1340I-delQ (data not shown).

Because the temperature increase from 22°C to 40°C may far exceed physiological temperature change, peak current densities of WT-delQ and V1340I-delQ were also studied at 32°C and 37°C with a depolarization pulse protocol (20 ms at −25 mV from a holding potential of −100 mV) in the same cell. Figure 4D shows superimposed current traces obtained from the cells expressing WT-delQ or V1340I-delQ at 22°C, 32°C, and 37°C. The peak currents became larger with the increase of temperature in the WT-delQ. However, the fold increase was significantly lower in the V1340I compared to the WT-delQ. Figure 4E shows bar graphs of WT-delQ and V1340I-delQ peak current densities at 3 different temperatures.

Effects of V1340I on time-dependent parameters

The role of time-dependent parameters in the pathophysiological mechanisms of BrS was studied.[18,25] Figure 5A shows the recovery from fast inactivation examined in the cells expressing WT-delQ or V1340I-delQ at 22°C and 40°C. The recovery time-course was studied using a double-pulse protocol. The currents at the test pulse were normalized by the currents at the pre-pulse, and plotted against the interval between the 2 pulses. The data were fitted with a double exponential function. Although there was no significant difference of the time constant between WT-delQ and V1340I-delQ at 22°C, the fast components of the recovery time-course were significantly faster in V1340I-delQ than WT-delQ at 40°C (Table 1).

The direct transition from the closed state to the inactivation state without channel opening (closed-state inactivation) has been recognized,[25] and therefore, closed-state inactivation kinetics were studied using pre-pulse protocols. The peak currents at the test pulse were normalized by the maximal currents, and plotted against the pre-pulse intervals (Figure 5B). The data were fitted with a single exponential function. At 22°C, the time course of closed-state inactivation was comparable between the WT-delQ and the V1340I-delQ. On the contrary, the transition from the closing state to the inactivation state was significantly slower in the V1340I than the WT at 40°C (Table 1). These results suggest that hyperthermia might increase the channel availability in the V1340I-delQ mutant after depolarization compared to the WT-delQ at hyperthermic state.

Discussion

In this study, we report a novel *SCN5A* mutation (V1340I) identified in a BrS patient with worsening arrhythmias during febrile illness. Further analysis of the effect of the mutation shows that background sodium channel variants may play important roles in the pathophysiology of BrS.

Possible underlying mechanisms for susceptibility to fever

Several mechanisms have been proposed to explain the pathophysiology of fever-induced BrS or the BrS-type ECG changes. Dumaine et al.[18] first reported that hyperthermia can affect the biophysical properties of the first mutant sodium channel (T1620M) identified in the BrS patients. They showed that the whole-cell current decay of T1620M was faster than the WT, and that T1620M shifted the I–V curve toward positive at 32°C. Mok et al.[19] reported that

hyperthermia can reduce the window currents due to the shift of voltage-dependent kinetics toward negative in an SCN5A mutant, (H681P), but not in the WT. Keller et al.[20,21] identified multiple SCN5A mutations in BrS patients whose phenotypes were augmented by fever. They proposed that the marked reduction of the basal peak current densities by L325R and R535X-*SCN5A* mutations might lead to the loss of the AP dome at high temperature (42°C) using the Luo-Rudy mathematical models in conjunction with 6-state Markovian models.[20] The same investigator reported that a *SCN5A* mutation, F1344S, reduced the current densities and shifted the voltage-dependent activation kinetics at 23°C, and that F1344S further shifted the activation curve toward positive by 8 mV at 40.5°C.[21] Very recently, Morita et al.[26] showed that hyperthermia can exaggerate the intramural AP dispersion leading to BrS-type ECG change using canine tissue models. Although they proposed that the transient outward potassium currents (I_{to}) can be another mediator of the fever-induced ECG phenotype, they concluded that the hyperthermic effects on the sodium channels may remain the main mechanisms of fever-induced BrS.

Our study has elucidated some novel pathophysiological mechanisms in fever-induced BrS. Although the current density of the V1340I-delQ was similar to the WT-delQ at 22°C, the V1340I-delQ was found to generate significantly smaller currents compared to the WT-delQ at 32°C, 37°C, and 40°C (Figures 4B and 4C). Interestingly, the temperature coefficient (Q_{10}) of V1340I-delQ is significantly smaller than the WT-delQ based on the current density measurement at 22°C and 37°C (equation: $Q_{10} = (I_{37°C} / I_{22°C})^{[10/(37-22)]}$; WT-delQ, 1.77 ± 0.39, n = 6; V1340I-delQ, 1.27 ± 0.18, n = 7, $P < .05$). Although direct comparison of Q_{10} in our study and other studies might not be feasible because of the difference in expression systems, used parameters, and temperature range, the Q_{10} of WT-delQ was similar to those reported in other studies (~2.0).[20,27] Keller et al.[20] suggested that Q_{10} values of the current density are dependent on the Q_{10} parameters of the activation and inactivation transition rates in the Luo-Rudy model. Thus, it is reasonable to speculate that V1340I mutation might also change the Q_{10} of transition rates in SCN5A-delQ.

Surprisingly, the V1340I-SCN5A did not show significant currents even though the channels were expressed in the plasma membrane (Figure 3E). If we assume that the composition of the sodium channel variants in human hearts are 35% SCN5A and 65% SCN5A-delQ, as suggested by Makielski et al.,[22] the proband's heart might express 4 different types of sodium channels at the following ratio: 17.5% WT-SCN5A, 17.5% V1340I-SCN5A, 32.5% WT-delQ, and 32.5% V1340I-delQ. If this is the case, the total sodium currents generated in the patient's cardiomyocytes might be reduced by 17.5% compared to normal subjects at baseline. This could account for his ECG phenotype in the afebrile state.

At high temperature, the V1340I-delQ decreases the peak currents by 46% compared to the WT-delQ. This leads to more than a 50% reduction of the total sodium currents because the total inward sodium currents were, indeed, decreased at 40°C compared to 22°C even for the WT sodium channels due to the acceleration of current decay.[18] This further decrease of the sodium currents by the V1340I mutant during the hyperthermic state might exaggerate the loss of the AP dome. In addition, our data showed that the V1340I-delQ's recovery time-course from fast inactivation was significantly faster than the WT-delQ, which might contribute to the maintenance of the arrhythmia circuits. Taken together, these data suggest that the biophysical modifications of sodium channels due to the V1340I mutation could, in part, account for the proband's clinical phenotypes.

However, one issue is that the father of the proband, a carrier of V1340I, has been seemingly healthy and never had any BrS symptoms such as syncope or ventricular arrhythmias. Although this phenomenon, described as low or incomplete penetrance, has been previously reported in BrS,[28] the underlying mechanisms for low penetrance have not yet been fully elucidated.

Possible explanations for our case are: (1) the proband but not his father carries unidentified BrS susceptibility gene(s), and/or (2) the father but not the proband carries unknown genetic variant(s) that can rescue or mitigate the BrS phenotype and restore the sodium channel dysfunctions caused by SCN5A gene defects. Thus, further genetic screenings including ion channel modifier genes (e.g., TCAP and SNTA1) are warranted to address this issue.[23]

How does the SCN5A variant contribute to the modification of $hNa_v1.5$?

Recently, the role of sodium channel variants and common polymorphisms in the regulation of $hNa_v1.5$ have gained much more attention because it may affect the clinical outcomes of not only the patients who suffer from arrhythmias but also a large number of individuals in general populations.[29,30,31] Therefore, some scientists, including us, sought to investigate the biophysical modifications of $hNa_v1.5$ by SCN5A backgrounds. For example, Tan et al.[24] reported that common SCN5A polymorphisms, S524Y and H558R, generated marked diminished currents in the SCN5A background compared to the currents in the SCN5A-delQ background. The same group also reported that G1406R, a mutation identified in a BrS patient, showed markedly reduced currents in the SCN5A background but not in the SCN5A-delQ background. Their immunostaining study elucidated that G1406R caused a trafficking defect that was rescued by mexiletine treatment.[32] However, in our study, a defective trafficking pattern may not sufficiently explain the underlying mechanisms because the V1340I-SCN5A channels were expressed in the plasma membrane (Figure 3E). Because little is known about the role of cytoplasmic loops of the $Na_v1.5$ except the one between DIII and DIV, we have no clear explanation of why Q1077 can drastically affect the V1340I and other SCN5A polymorphisms. One speculative mechanism is that the interaction between Q1077 and these mutations may interfere the unbinding of the IFM motif located in the cytoplasmic loop between DIII and DIV (i.e., inactivation gating machinery) from the pore lesion by altering the tertiary structure of the channel and/or direct interactions, which might result in the drastic decrease of the channel open probability. However, further electrophysiological studies using single-channel recordings and biochemical studies in conjunction with crystallography are needed to answer these questions, and this is beyond the scope of this study.

Study limitations

Several significant limitations must be considered when trying to link our data to the clinical manifestations: (1) the data were obtained using in vitro experiments using non-cardiomyocyte cells that only express sodium channel α-and β_1-subunits, a different model from the actual environment in human hearts; (2) the pulse protocols used to study ion channel gating kinetics were far different from physiological action potentials; (3) there is no evidence that temperature changes in in vitro cell lines correspond to those occurring in human heart; and (4) the effects of hyperthermia on other ion channels (e.g., transient outward potassium currents) were not considered. However, our data suggest that febrile illness and sodium channel variants can be important factors that can modify BrS phenotypes.

Conclusion

We have identified a novel *SCN5A* mutation, V1340I, in a patient who presented with frequent ventricular arrhythmias during febrile illness. The electrophysiological study using patch-clamp techniques revealed that V1340I was essentially nonfunctional in the SCN5A background, and significantly reduced sodium currents in the SCN5A-Q1077del (delQ) background at high temperature. In addition, V1340I-delQ accelerated the recovery time from fast inactivation. These biophysical modifications of $hNa_v1.5$ by V1340I predispose to ventricular arrhythmias during febrile illness.

Acknowledgment

The authors thank the patient and family members who participated in this study. The authors also thank Shahrzad Abbasi for her technical assistance.

Dr. Ai was the recipient of the Roderick D. MacDonald General Research Fund Awards. Dr. Towbin was supported by Texgen and the Texas Children's Foundation Chair in Pediatric Cardiac Research.

References

1. Brugada P, Brugada J. Right bundle branch block, persistent ST segment elevation and sudden cardiac death: a distinct clinical and electrocardiographic syndrome. J Am Coll Cardiol 1992;20:1391–1396. [PubMed: 1309182]
2. Brugada J, Brugada P. Further characterization of the syndrome of right bundle branch block, ST segment elevation, and sudden cardiac death. J Cardiovasc Electrophysiol 1997;8:325–331. [PubMed: 9083883]
3. Brugada J, Brugada R, Brugada J. Right bundle-branch block and ST-segment elevation in leads V1 through V3: a marker for sudden death in patients without demonstrable structural heart disease. Circulation 1998;97:457–460. [PubMed: 9490240]
4. Alings M, Wilde A. "Brugada" syndrome: clinical data and suggested patho-physiological mechanism. Circulation 1999;99:666–673. [PubMed: 9950665]
5. Antzelevitch C, Brugada P, Brugada J, Brugada R, Towbin JA, Nademanee K. Brugada syndrome: 1992–2002: a historical perspective. J Am Coll Cardiol 2003;41:1665–1671. [PubMed: 12767644]
6. Antzelevitch C, Brugada P, Brugada J, et al. Brugada syndrome: a decade of progress. Circ Res 2002;91:1114–1118. [PubMed: 12480811]
7. Antzelevitch C. The Brugada syndrome: ionic basis and arrhythmia mechanisms. J Cardiovasc Electrophysiol 2001;12:268–272. [PubMed: 11232628]
8. Coronel R, Casini S, Koopmann TT, et al. Right ventricular fibrosis and conduction delay in a patient with clinical signs of Brugada syndrome: a combined electrophysiological, genetic, histopathologic, and computational study. Circulation 2005;112:2769–2777. [PubMed: 16267250]
9. Frustaci A, Priori SG, Pieroni M, et al. Cardiac histological substrate in patients with clinical phenotype of Brugada syndrome. Circulation 2005;112:3680–367. [PubMed: 16344400]
10. Amin AS, Meregalli PG, Bardai A, Wilde AA, Tan HL. Fever increases the risk for cardiac arrest in the Brugada syndrome. Ann Intern Med 2008;149:216–218. [PubMed: 18678856]
11. Junttila MJ, Gonzalez M, Lizotte E, et al. Induced Brugada-type electrocardiogram, a sign for imminent malignant arrhythmias. Circulation 2008;117:1890–1893. [PubMed: 18391123]
12. Kalra S, Iskandar SB, Duggal S, Smalligan RD. Fever-induced ST-segment elevation with a Brugada syndrome type electrocardiogram. Ann Intern Med 2008;148:82–84. [PubMed: 18166764]
13. Aramaki K, Okumura M, Shimizu M. Chest pain and ST elevation associated with fever in patients with asymptomatic Brugada syndrome: fever and chest pain in Brugada syndrome. Int J Cardiol 2005;103:338–339. [PubMed: 16098400]
14. Saura D, García-Alberola A, Carrillo P, Pascual D, Martínez-Sánchez J, Valdés M. Brugada-like electrocardiographic pattern induced by fever. Pacing Clin Electrophysiol 2002;25:856–859. [PubMed: 12049381]
15. Ortega-Carnicer J, Benezet J, Ceres F. Fever-induced ST-segment elevation and T-wave alternans in a patient with Brugada syndrome. Resuscitation 2003;57:315–317. [PubMed: 12804811]
16. Patruno N, Pontillo D, Achilli A, Ruggeri G, Critelli G. Electrocardiographic pattern of Brugada syndrome disclosed by a febrile illness: clinical and therapeutic implications. Europace 2003;5:251–255. [PubMed: 12842639]
17. Dinckal MH, Davutoglu V, Akdemir I, Soydinc S, Kirilmaz A, Aksoy M. Incessant monomorphic ventricular tachycardia during febrile illness in a patient with Brugada syndrome: fatal electrical storm. Europace 2003;5:257–261. [PubMed: 12842640]
18. Dumaine R, Towbin JA, Brugada P, et al. Ionic mechanisms responsible for the electrocardiographic phenotype of the Brugada syndrome are temperature dependent. Circ Res 1999;85:803–809. [PubMed: 10532948]

19. Mok NS, Priori SG, Napolitano C, et al. A newly characterized SCN5A mutation underlying Brugada syndrome unmasked by hyperthermia. J Cardiovasc Electrophysiol 2003;14:407–411. [PubMed: 12741714]

20. Keller DI, Rougier JS, Kucera JP, et al. Brugada syndrome and fever: genetic and molecular characterization of patients carrying SCN5A mutations. Cardiovasc Res 2005;67:510–519. [PubMed: 15890323]

21. Keller DI, Huang H, Zhao J, et al. A novel SCN5A mutation, F1344S, identified in a patient with Brugada syndrome and fever-induced ventricular fibrillation. Cardiovasc Res 2006;70:521–529. [PubMed: 16616735]

22. Makielski JC, Ye B, Valdivia CR, et al. A ubiquitous splice variant and a common polymorphism affect heterologous expression of recombinant human SCN5A heart sodium channels. Circ Res 2003;93:821–828. [PubMed: 14500339]

23. Wu G, Ai T, Kim JJ, et al. Alpha-1syntrophin mutation and the long-QT syndrome: a disease of sodium channel disruption. Circ Arrhythmia Electrophysiol 2008;1:193–201.

24. Tan BH, Valdivia CR, Rok BA, et al. Common human SCN5A polymorphisms have altered electrophysiology when expressed in Q1077 splice variants. Heart Rhythm 2005;2:741–747. [PubMed: 15992732]

25. Shirai N, Makita N, Sasaki K, et al. A mutant cardiac sodium channel with multiple biophysical defects associated with overlapping clinical features of Brugada syndrome and cardiac conduction disease. Cardiovasc Res 2002;53:348–354. [PubMed: 11827685]

26. Morita H, Zipes DP, Morita ST, Wu J. Temperature modulation of ventricular arrhythmogenicity in a canine tissue model of Brugada syndrome. Heart Rhythm 2007;4:188–197. [PubMed: 17275755]

27. Benndorf K. Properties of single cardiac Na channels at 35°C. J Gen Physiol 1994;104:801–820. [PubMed: 7876824]

28. Priori SG, Napolitano C, Gasparini M, et al. Clinical and genetic heterogeneity of right bundle branch block and ST-segment elevation syndrome: a prospective evaluation of 52 families. Circulation 2000;102:2509–2515. [PubMed: 11076825]

29. Viswanathan PC, Benson DW, Balser JR. A common SCN5A polymorphism modulates the biophysical effects of an SCN5A mutation. J Clin Invest 2003;111:341–346. [PubMed: 12569159]

30. Poelzing S, Forleo C, Samodell M, et al. SCN5A polymorphism restores trafficking of a Brugada syndrome mutation on a separate gene. Circulation 2006;114:368–376. [PubMed: 16864729]

31. Splawski I, Timothy KW, Tateyama M, et al. Variant of SCN5A sodium channel implicated in risk of cardiac arrhythmia. Science 2002;297:1333–1336. [PubMed: 12193783]

32. Tan BH, Valdivia CR, Song C, Makielski JC. Partial expression defect for the SCN5A missense mutation G1406R depends on splice variant background Q1077 and rescue by mexiletine. Am J Physiol Heart Circ Physiol 2006;291:H1822–H1828. [PubMed: 16632547]

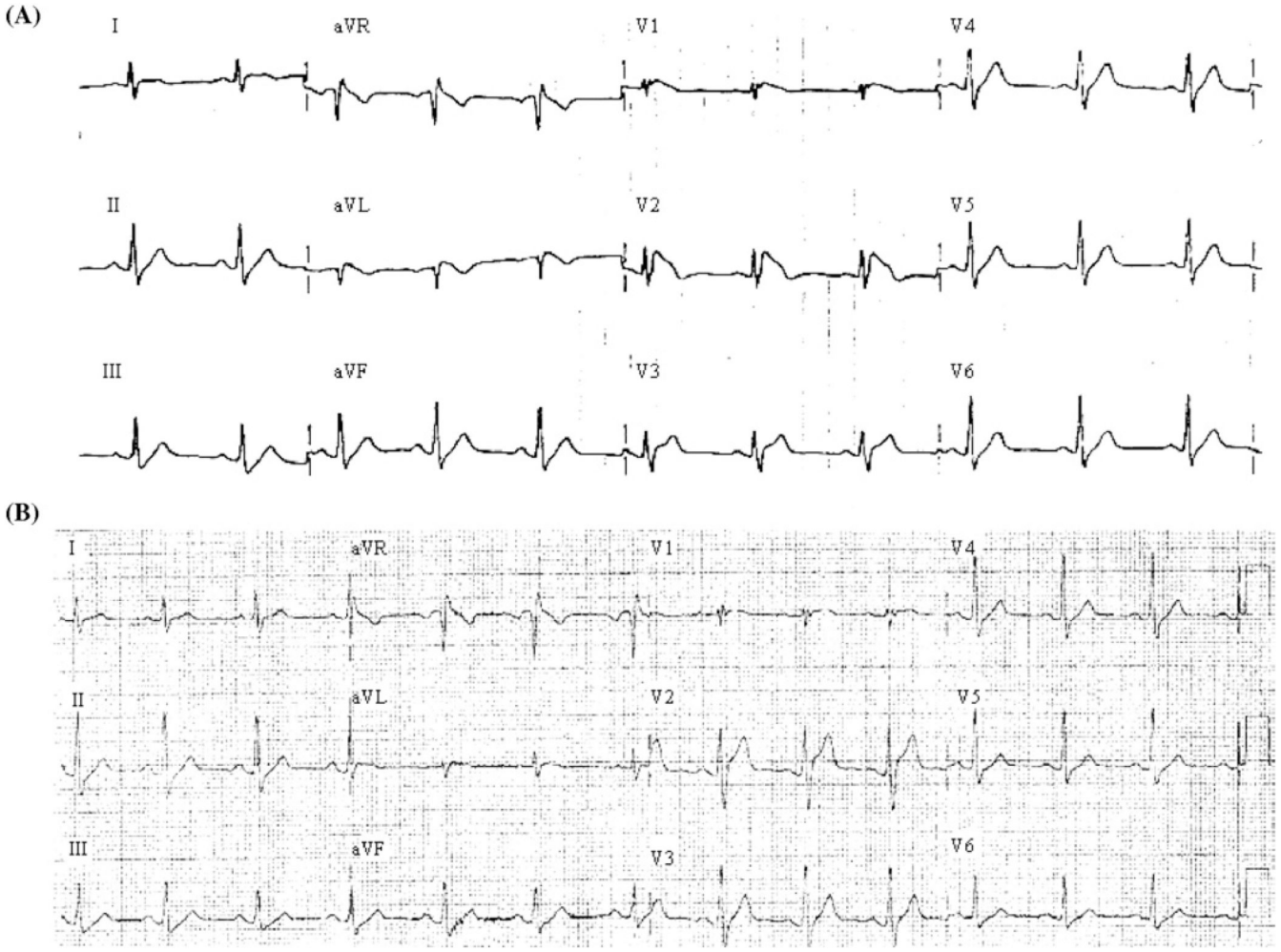

Figure 1.

ECG phenotypes. (**A**) The 12-lead ECG at the time of diagnosis shows the coved-type Brugada sign, the ST-segment elevation in the right precordial leads (V_1 and V_2). (**B**) The 12-lead ECG in the afebrile state shows incomplete RBBB and mild ST-segment elevation in V_1 lead. ECG = electrocardiographic; RBBB = right bundle branch block.

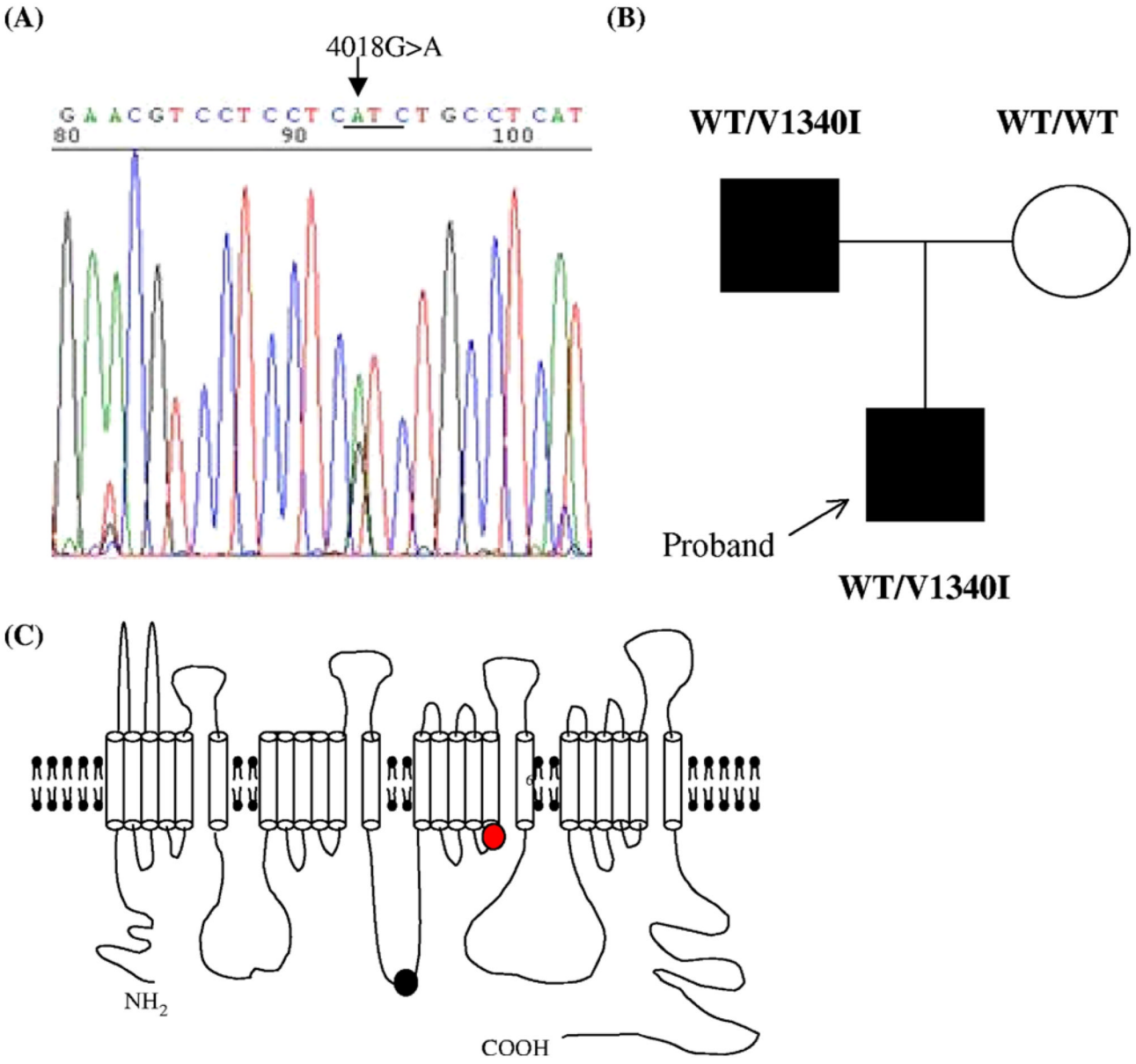

Figure 2.

Genetic analysis. (**A**) DNA sequence analysis shows a G to A nucleotide change in *SCN5A*, resulting in the amino acid substitution V1340I. (**B**) Family pedigree. The black filled square indicates the career of V1340I. (**C**) A schematic illustration of sodium channel topology. The red circle indicates the relative position of the V1340I mutation in the S5 of the domain III. The black circle indicates the position of Q1077.

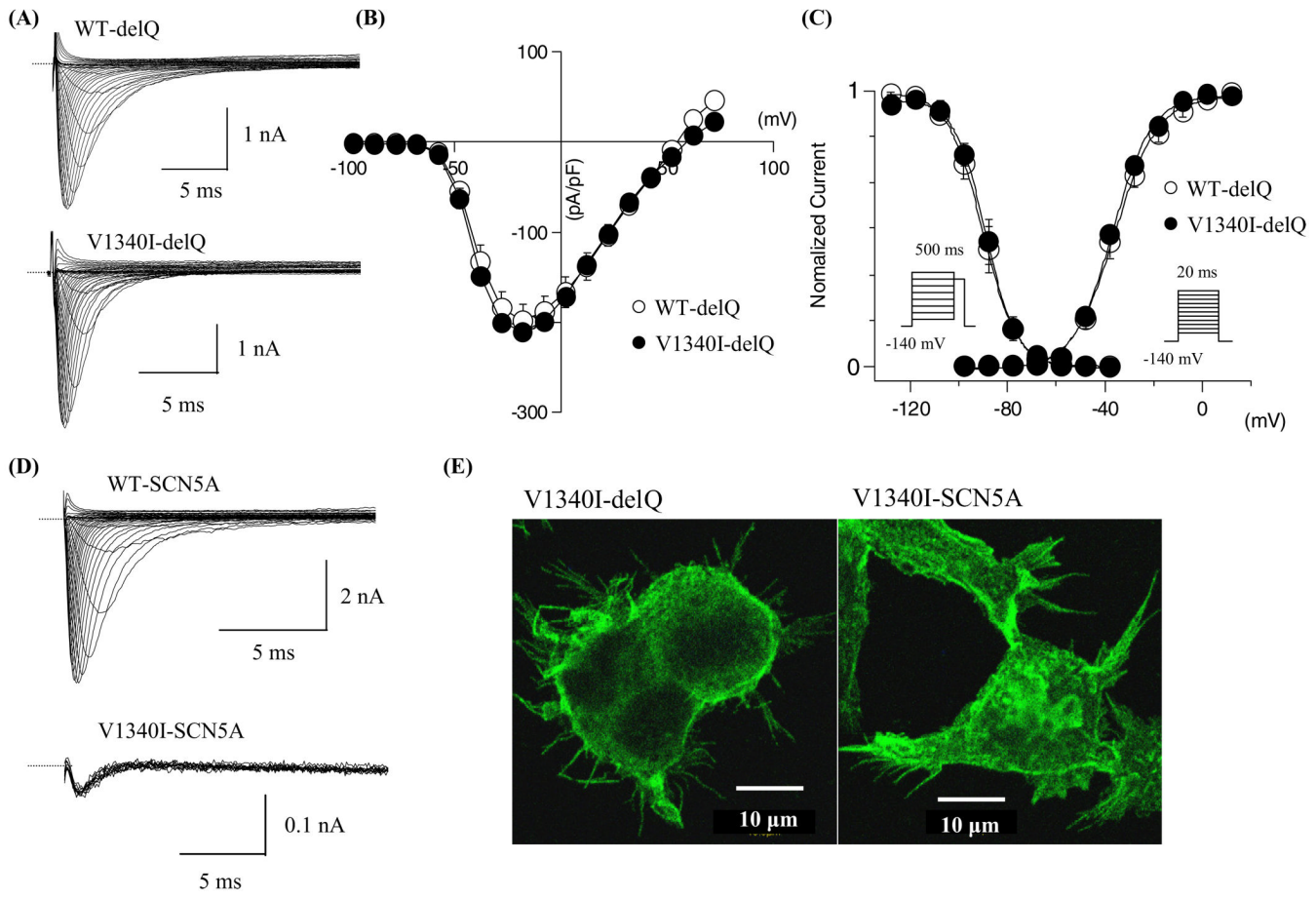

Figure 3.

Gating kinetics of WT and mutant sodium channels at 22°C. (**A**) Superimposed macroscopic sodium currents obtained from the cells expressing WT-delQ and V1340I-delQ. The currents were induced by step-pulse protocols from a holding potential of −140 mV at 22°C. (**B**) I–V relationships at 22°C. (C) Voltage-dependent kinetics of the peak conductance and the steady-state fast inactivation at 22°C. Conductance G(V) was calculated by the equation: $G(V) = I/(V_m - E_{rev})$, where I is the peak currents, E_{rev} is the measured reversal potential, V_m is the membrane potential. The normalized peak conductance was plotted against the membrane potentials. Steady-state inactivation was estimated by 500-ms pre-pulse protocols from a holding potential of −140 mV. Normalized peak currents were plotted against the pre-pulse membrane potentials. Data were fitted with the Boltzmann equation: $y = [1 + \exp((V_h - V_m)/k)]^{-1}$, where *y* represents variables; V_h, midpoint; *k*, slope factor; V_m, membrane potential. Data were represented as mean ± SD. (**D**) Superimposed current traces of the WT-SCN5A obtained by step-pulse protocols at 22°C (upper panel). Superimposed current traces of V1340I-SCN5A obtained by repetitive depolarization pulses (20 ms at −10 mV every 15 s) from a holding potential of −140 mV at 22°C (lower panel). Notice that V1340I-SCN5A generated very small currents. (**E**) Fluorescent microscopic images of the HEK-293 cells stably expressing V1340I-delQ or V1340I-SCN5A. WT = wild type.

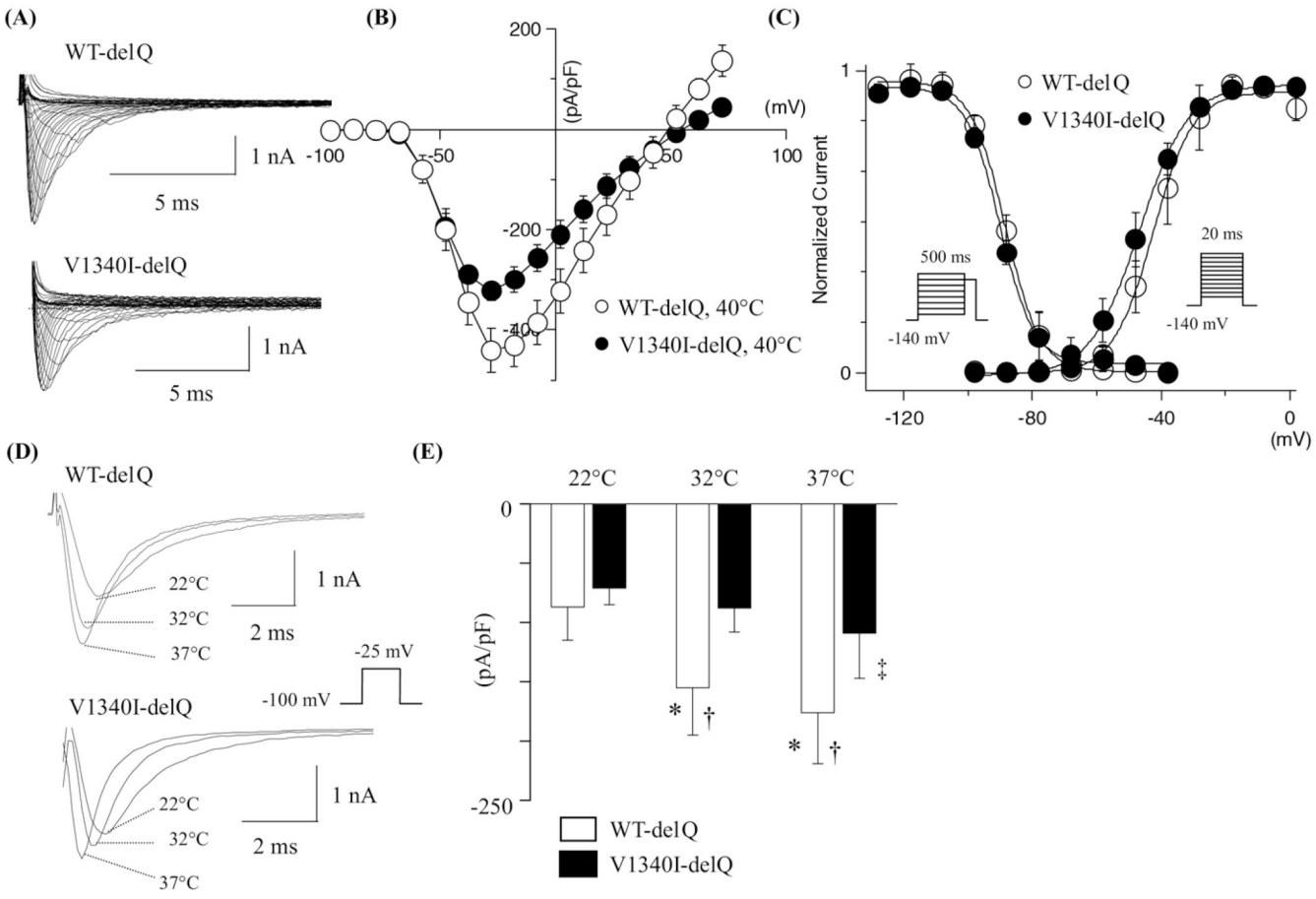

Figure 4.

Hyperthermic effects on the gating kinetics of WT-delQ and V1340I-delQ. (**A**) Superimposed whole-cell current traces induced by step-pulse protocols from a holding potential of −140 mV at 40°C. (**B**) I–V relationships at 40°C. (**C**) Voltage dependency of the steady-state activation and the fast inactivation at 40°C. (**D**) Representative superimposed current traces obtained from the cells expressing WT-delQ or V1340I-delQ at 3 different temperatures. The currents were induced with a depolarization pulse protocol. (**E**) Bar graphs of WT-delQ and V1340I-delQ current densities at various temperatures. Data are presented as mean ± SD. **P* <.005 vs. 22°C; †*P* <.005 vs. V1340I; ‡*P* <.01 vs. 22°C.

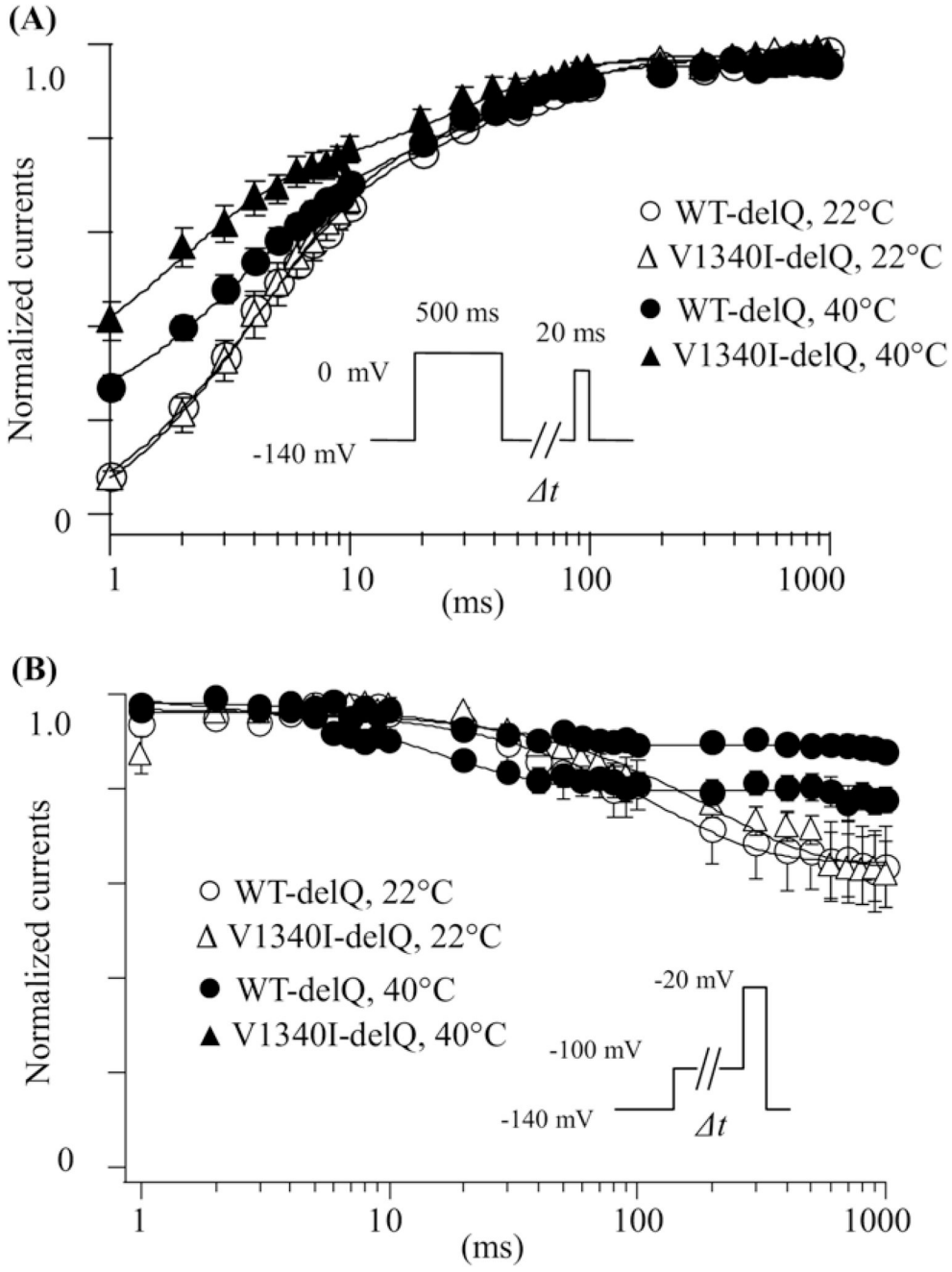

Figure 5.

Time-dependent parameters of WT-delQ and V1340I-delQ. (**A**) Recovery from fast inactivation estimated by a double-pulse protocol. Cells were depolarized at 0 mV for 500 ms from a holding potential of −140 mV, then stepped to −140 mV for various duration before the 2nd pulse (20 ms at −20 mV). Fractional recovery was calculated as a ratio of peak currents at the second pulse. The time course was fitted with a double-exponential function: I(t)/Imax = $C - A_f \times \exp(-t/\tau_f) - A_s \times \exp(-t/\tau_s)$, where t is the recovery time, A_f and A_s are the fraction of fast and slow components, τ_f and τ_s are the time constants of fast and slow components of recovery. (**B**) Closed-state inactivation. Membrane potential was held at −100 mV for various durations (Δt) from a holding potential of −140 mV before the test pulse (20 ms at −20 mV).

The normalized currents by the maximal currents (t = 1 ms) were plotted against Δt. Data were represented as mean ± SE.

Table 1

Gating kinetics of WT and V1340I§

	22°C		40°C	
	WT-delQ	**V1340I-delQ**	**WT-delQ**	**V1340I-delQ**
Current density (pA/pF)	(7)	(7)	(7)	(7)
	198.7 ± 18.1*	210.2 ± 5.1*	450.6 ± 45.9	330.4 ± 15.7†
Activation	(7)	(7)	(7)	(7)
V_h (mV)	−36.0 ± 1.9‡	−37.1 ± 0.9‡	−45.1 ± 1.9	−46.5 ± 2.9
k	7.9 ± 0.4*	7.8 ± 0.9‡	4.3 ± 0.3	6.2 ± 0.6†
Fast inactivation	(9)	(9)	(9)	(9)
V_h (mV)	−89.9 ± 1.8	−86.3 ± 1.3	−88.3 ± 1.7	−85.6 ± 1.7
k	5.7 ± 0.2	5.0 ± 0.4	4.3 ± 0.3	4.1 ± 0.6
Recovery from fast inactivation	(6)	(9)	(11)	(8)
τ_f (ms)	4.30 ± 0.45	4.44 ± 0.69*	3.28 ± 0.42	1.95 ± 0.27†
τ_s (ms)	48.0 ± 5.4	43.1 ± 3.5	40.4 ± 6.4	31.2 ± 5.4
A_f	0.77 ± 0.04*	0.83 ± 0.04*	0.54 ± 0.03	0.50 ± 0.06
A_s	0.29 ± 0.03	0.27 ± 0.02	0.30 ± 0.07	0.29 ± 0.02
Closed-state inactivation	(8)	(11)	(7)	(5)
τ (ms)	146.3 ± 28.1*	137.7 ± 18.4*	16.7 ± 2.2	26.9 ± 3.5†
A	0.34 ± 0.09	0.29 ± 0.03*	0.20 ± 0.03	0.09 ± 0.01†
Current decay	(9)	(10)	(6)	(9)
τ_f (ms)	1.26 ± 0.08*	1.35 ± 0.13*	0.21 ± 0.03	0.26 ± 0.02
τ_s (ms)	6.54 ± 1.06‡	7.76 ± 1.14*	2.41 ± 0.45	2.07 ± 0.18

The numbers in the parentheses represent number of patches.

A_f = the fraction of fast components; A_S = the fraction of slow components; k = slope factor; τ_f = time constants of fast components of recovery and current decay; τ = the time constants of development of slow inactivation; τ_S = the time constants of slow components of recovery and current decay; V_h = the membrane potential for half maximal activation or inactivation; WT = wild type.

*P <.01 22°C vs. 40°C.

†P <.05 V1340I vs. WT.

‡P <.05 22°C vs. 40°C.